Simultaneous Flexural and Punching Strengthening of RC Slabs according to a New Hybrid Technique Using U-Shape CFRP Laminates

Joaquim A.O. Barros[1], Mohammadali Rezazadeh[2], João P.S. Laranjeira[3], Mohammad R.M. Hosseini[4], Mohammad Mastali[5], Honeyeh Ramezansefat[6]

ISISE, Dep. Civil Engineering, School Engineering, University of Minho, Campus de Azurém, 4800-058 Guimarães, PORTUGAL; [1]barros@civil.uminho.pt, [2]rzh.moh@gmail.com, [3]joaopslaranjeira@gmail.com, [4]hoseini_engineer@yahoo.com, [5] m.mastali@civil.uminho.pt , [6]honeyrscivil@gmail.com

ABSTRACT:

One of the main concerns related to flat reinforced-concrete (RC) slabs is the slab's punching capacity. Punching can occur not only due to a deficient transverse reinforcement, but also when the flexural capacity of the slab needs to be increased. To increase the flexural capacity, carbon-fiber-reinforced-polymer (CFRP) composites have been applied according to near-surface-mounted (NSM) or external-bonded-reinforcement (EBR) techniques, while for the punching strengthening CFRP reinforcements have been applied according to embedded-through-section (ETS) technique. To take advantage of strengthening benefits of the NSM and ETS techniques, in the present paper a new type of CFRP laminate of U-shape is used by adopting a novel hybrid technique for the simultaneous flexural and punching strengthening of existing RC slabs. Besides, this hybrid technique aims to provide a better bond performance for the ETS and NSM CFRPs by improving the anchorage conditions. Moreover, a higher resistance to the susceptibility of occurrence of other premature failure modes, like concrete cover delamination, is offered by using this hybrid technique. A 3D nonlinear finite-element (FE) model is developed to simulate the experimental tests by considering the nonlinear behavior of the constituent materials. The experimental program and numerical model are described, and the relevant results are analyzed.

Keywords: Flexural strengthening; punching shear strengthening; RC slabs; CFRP reinforcement; FE model.

1. INTRODUCTION

In the residential and commercial buildings, there are many structures composed of flat reinforced concrete (RC) slabs supported by RC columns with relatively high span length. In these types of the structures, in spite of their economic advantages, one of the serious concerns from the design point of view is the occurrence of punching failure, since it is a sudden and brittle failure, sometimes conducting to the global collapse of the building [1-4]. This punching failure occurs due to the formation and propagation of a concrete fracture surface initiated from the column-slab interface on the slab compressive fiber and propagating through the depth of the slab in an inclined direction away from the column [5]. Therefore, the concrete fracture surface of punching failure has the form of frustum of a pyramid for conventional square and circular RC columns [5]. For the design purpose of this type of ~~the~~ structures, a certain punching reinforcement ratio should be adopted around the column to provide the required punching resistance, in order to assure the occurrence of ductile flexural failure mode.

On the other hand, existing flat RC slabs may become vulnerable during their lifetime due to several reasons, such as: application of higher permanent and/or live load than the structure's initial design loads; degradation of their material properties; design or construction errors; and damage due to earthquake. These structures should be repaired or strengthened to ensure proper performance for the current service load demands [6]. Carbon Fiber reinforced polymer (CFRP) reinforcement is one of the most recent type of material for the punching strengthening of flat RC slabs.

Regarding the punching strengthening purposes using CFRP composite materials, they have been applied to RC slabs to be strengthened by using either externally bonded reinforcement (EBR), near surface mounted (NSM), or embedded through section (ETS) techniques. The EBR technique is based on applying CFRP sheets/laminates on the tensile surface of RC slabs, while according to the NSM technique, CFRP laminates/rods are inserted into the grooves pre-executed on the tensile surface of RC slabs. In both EBR and NSM techniques the CFRP systems are applied for the flexural strengthening. Studies have shown that the NSM technique offers higher strengthening effectiveness than the EBR technique due to higher confinement to the CFRP composite materials provided by the surrounding concrete [2, 7-9]. The ETS technique has been used with considerable success for the shear strengthening of RC beams, where FRP or steel bars are installed into vertical or inclined holes drilled through the core of the beam's cross section [10]. In case of RC slabs the ETS is used to increase their punching capacity by introducing FRP/steel reinforcements into vertical or inclined holes drilled through the depth of the existing slab around the column [5, 11, 12]. The punching strengthening efficiency of the ETS technique is quite dependent of the geometric arrangement of the punching reinforcements [5]. This geometric arrangement of the shear reinforcements can, moreover, cause a punching failure outside or within the corresponding ETS shear reinforced zone in the strengthened RC slabs [5].

The available research evidences that the use of CFRP reinforcement applied flexurally according to either EBR or NSM technique, in addition of increasing the flexural capacity of existing RC slabs, improves moderately the punching strength, which is not enough in some cases [2, 13-15]. The improvement of the punching strength of the existing RC slab using the EBR and NSM CFRPs increases with the corresponding compressive strength of the concrete, as well as when the percentage of existing longitudinal steel reinforcement is relatively low [13, 14]. Besides, regarding the CFRP reinforcement applied according to ETS technique for the shear strengthening purposes, these ETS CFRPs have almost no effect on the flexural load carrying capacity of the strengthened slabs. Moreover, the debonding of ETS CFRPs, as dominant failure mode due to the small depth of slabs, is a concern from strengthening design point of view using ETS technique [11]. Accordingly, developing a new strengthening system, capable of assuring simultaneously flexural and punching strengthening of RC slabs, with the aim of improving the strengthening performance of the separate use of NSM and ETS techniques for the flexural and punching strengthening applications, is still a challenge that needs to be addressed.

The current study aims to experimentally evaluate the potentialities of a novel hybrid technique for the simultaneous flexural and punching strengthening of existing RC slabs. This hybrid strengthening technique combines the NSM technique for the flexural strengthening and ETS technique for the punching strengthening purposes in the same application using innovative U-shape CFRP laminates. In other words, the central part of this U-shape laminate is applied on the tensile surface of RC slab according to the NSM technique for the flexural strengthening and its extremities are used for the punching strengthening according to the ETS technique. In fact, this hybrid technique aims to provide, in addition to a simultaneous flexural and punching strengthening application, a better bond performance for the ETS and NSM CFRPs by increasing the relevant bonded length and anchorage mechanisms. Moreover, a higher resistance to the susceptibility of occurring other premature failure modes, like concrete cover delamination failure (concrete rip-off failure), is offered by using the new U-shape CFRP laminates, since the extremities of the NSM CFRP laminates are anchored into the slab according to the ETS technique.

Due to the complexities of punching failure in RC slabs, besides the available experimental research related to the punching strengthening of RC slabs, numerical analyses are also necessary to better analyze the influence of the several parameters on the strengthening efficiency of the available techniques in this context. However, modeling numerically the relevant nonlinear phenomena involved in the behavior of RC slabs failing in punching requires sophisticated constitutive models, which justifies the relatively small number of publication in this domain [16-18]. This level of sophistication increases when the slab is punching strengthened with FRP systems. Therefore, another challenging of the present work is to verify the applicability of a 3D multidirectional smeared crack model [19] in the simulation of RC slabs punching strengthened with the hybrid technique and using the new CFRP laminates. The good predictive performance of this model was already demonstrated in the simulation of RC beams failing in shear [20].

2. EXPERIMENTAL PROGRAM

The experimental program was composed of three full-scale flat RC slabs. One of the RC slabs was kept unstrengthened, constituting the control slab (designated as UnStr. slab), while the other two slabs were strengthened adopting different CFRP reinforcement ratios (CFRP configuration A and B) aiming to evaluate the influence of this ratio on the strengthening performance.

2.1. Slabs and Test Setup

The loading configuration and support conditions of the tested slabs are schematically indicated in Fig. 1, where this figure shows that these slabs were supported by twelve dywidag steel bars of 35 mm diameter. The slabs were monotonically loaded in the center, using a steel plate of $200 \times 200 \times 50$ mm^3 placed between the slab and the actuator by imposing a displacement rate of 0.6 mm/min. Fig. 2, moreover, indicates the geometry and steel reinforcement details of the slabs of the experimental program. A relatively low ratio was adopted for the flexural steel reinforcement of the RC slabs, in order to justify the interest of using CFRP laminates for increasing the flexural capacity of these slabs.

A tensile flexural steel reinforcement ratio (ρ_{sl}) of 0.53% (using $\phi 10$) was applied in the top zone of the slabs of this experimental program, while in the bottom compressive zone a reinforcement ratio of 0.34% was adopted (using $\phi 8$). These flexural steel reinforcements were symmetrically disposed in both directions, and adopted in all the tested slabs (see Fig. 2). According to the Eurocode 2, the ρ_{sl} should be calculated as the mean value in a slab strip of $e+6.d$ in each direction, where e is the edge of the cross section of the column (the loading cross section in the present experimental program that was 200 mm) and d is the internal arm of the longitudinal tensile steel bars (see Fig. 2, $d=125$ mm) [21, 22].

2.2. Flexural and Punching Strengthening System

In the current experimental program, for the simultaneous flexural and punching strengthening of RC slabs, the conventional and new U-shape CFRP laminates were applied on the tensile surface of the RC slabs according to the NSM and proposed hybrid techniques, respectively. According to the hybrid technique, the central part of the U-shape CFRP laminates is applied according to the NSM technique for the flexural strengthening purpose, while its extremities are used for the shear strengthening according to the ETS technique.

Regarding the flexural strengthening according to the hybrid technique, the U-shape CFRP laminates provide the benefits of anchoring (with the length of L_{af} in Fig. 3) the extremities of the NSM CFRP laminates into the RC structure using the ETS technique, which can be considered as the development length for the NSM part. In this regards, according to the recommendations of ACI 440.2R [23], the required development length is determined by $l_{db} \geq \left(a_b.b_b.f_{fe}\right) / \left(2.(a_b+b_b).\tau_b\right)$, where a_b and b_b are the thickness and height of the laminate's cross section, f_{fe} and τ_b are the effective tensile stress of CFRP which is 0.7 of its ultimate tensile strength and the average bond strength, respectively. By considering for a_b, b_b, f_{fe} and τ_b the values of 1.4 mm, 10 mm, 2030 MPa, and 6.9 MPa, respectively, it was obtained $l_{db} \geq 180$ mm. The adopted value for the average bond strength (τ_b) was recommended by [24] for the CFRP laminates applied according to the NSM technique. However, in the experimental program, the extremity of the U-shape CFRPs (as the development length for the corresponding NSM part) is applied according to the ETS technique, providing a higher bond strength, while the value of 6.9 MPa was adopted due to the uncertainty in terms of the τ_b value. The anchorage benefits for the U-shape CFRPs consist of reducing the susceptibility of occurrence of premature failure modes (like concrete cover delamination) and increasing the resistance on the CFRP debonding failure in its extremity bonded zones (assuming a critical CFRP bonded length of L_{bf}^{cr} in Fig. 3), when compared to the only application of conventional NSM CFRPs for the flexural strengthening purposes.

Besides, for the purpose of shear strengthening according to the hybrid technique, the anchorage benefits for the extremity shear parts of U-shape CFRP laminates applied according to the ETS technique (assuming a critical CFRP bonded length of L_{bs}^{cr} in Fig. 3) can be provided by the central part of the U-shape CFRP laminates (with the length of L_{as} in Fig. 3) applied according to the NSM technique (see Fig. 3). These anchorage benefits are more highlighted in RC structures with relatively small depth (like RC flat slabs). Moreover, the extremities of U-shape CFRP laminates were applied adopting an inclined direction with a horizontal angle of 30° to provide additional improvements in terms of the bond performance of the ETS CFRPs. This inclination angle was adopted aiming to minimize the CFRP tensile stress concentrations in the bent zones, which was previously investigated by the authors [25].

Hence, two CFRP strengthening configurations, Str. A and Str. B, represented in Figs. 4 and 5, respectively, were adopted for the simultaneous flexural and punching strengthening of the RC slabs in this experimental program. These two strengthening configurations (A and B) were organized symmetrically in both directions with the aim of providing an almost similar flexural-shear strengthened zone with different CFRP strengthening ratio, as indicated in Fig. 6. For this purpose, the Str. A and Str. B were conceived to have an approximate CFRP reinforcement ratio of 0.1% and 0.2%, respectively (see Figs. 4 and 5). The adopted methodology to calculate these CFRP ratios was similar to the corresponding one for the longitudinal steel reinforcement ratio (as described in the previous section).

According to the adopted CFRP configurations, in the current experimental program CFRP laminates of 1.4×10 mm^2 cross sectional area were introduced into the grooves pre-executed on the concrete tensile surface of the RC slabs. However, in order to provide the possibility of applying CFRP laminates in two perpendicular directions on the tensile surface of RC slabs, two sets of grooves of different depth were executed for the installation of the CFRP laminates, one in the x direction with a cross section of 5×23 mm^2, and the other of 5×11 mm^2 cross section in the y direction. The grooves with higher depth were aligned with the tensile steel bars of larger concrete cover. To apply the extremities of the U-shape CFRP laminates according to the ETS technique, holes with a 30º inclination angle were executed through the slab cross section with a diameter of 11 mm.

In the Str. A configuration (Fig. 4), the conventional C4 and C5 laminates and the U-shape C2 and C3 laminates were introduced into the separate grooves with a distance of 60 mm. In the Str. B configuration (Fig. 5), the conventional C4 to C7 laminates were applied with a distance of 100 mm for the flexural strengthening, and the U-shape C2 and C3 laminates were placed at each side of the conventional NSM laminates C4 and C5, as represented in Fig. 5. It means that in the central part of these conventional laminates, where higher bending moments are expected, three laminates (one conventional and two U-shape laminates) were installed into the same groove according to the NSM technique (see Fig. 5). Accordingly, the groove width in the relevant central parts was increased to 10 mm. In both Str. A and Str. B configurations, L-shape CFRP laminates (instead of using U-shape laminates) were applied in the center of the slabs (Section A-A in Figs. 4 and 5) in the separate grooves due to the restrictions caused by the continuity effect of columns between floors in a real strengthening application (see Figs. 4 and 5).

For the Str. A and Str. B configurations, electric strain gauges (SG) were installed on NSM CFRP laminates according to the arrangements represented in Figs. 4 and 5 for measuring the tensile strains in the zones where these SGs were installed. The SG1 and SG2 were installed in the central part of the new types of laminates, while the SG3 to SG6 were placed in their inclined part, close to the transition zones of these laminates, as shown in Figs. 4 and 5.

2.3. Material Properties

The average values of the main properties of concrete, steel bars, and CFRP laminates are indicated in Table 1. The average compressive strength and Young's modulus of the concrete were evaluated from uniaxial compression tests on cylinders of 150 mm diameter and 300 mm height at the age of the slab tests (100 days). The uniaxial tensile tests of steel bars were carried out to characterize the tensile properties according to [26]. The tensile properties of the used CFRPs, consisting in CFK 150/2000 S&P laminates, were evaluated following the recommendations of [27]. The CFRP laminates were bonded to the surrounding concrete substrate by using S&P Resin epoxy adhesive of 220 and 55, the first one was applied in the groove zone where the laminates were installed according to the NSM technique, while the 55 type adhesive was used to fill the holes where the extremities of the U-shape laminates were inserted according to the ETS technique.

3. EXPERIMENTAL RESULTS

3.1. Load-deflection Curves

The relationship between the applied load and the deflection at the center of all the tested slabs is depicted in Fig. 7a, and the main relevant results of these responses are indicated in Table 2. Fig. 7b shows an increase of about 30% and 50% in terms of the maximum load carrying capacity for the slabs strengthened with CFRP configuration A (Str. A slab) and B (Str. B slab), respectively, when compared to the corresponding capacity of the UnStr. Slab. This figure, moreover, represents the strengthening efficiency in terms of load carrying capacity at concrete cracking, SLS conditions, and steel yield initiation stage for the Str. A and Str. B slabs, where the load capacities were normalized to the corresponding ones of the UnStr. Slab. For all the parameters analyzed in Fig. 7b, the slab strengthened with CFRP configuration B provided a higher load capacity than the slab strengthened using CFRP configuration A, due to the higher CFRP reinforcement ratio. In this figure, the criteria adopted to evaluate the load capacities at concrete cracking and steel yielding initiations was according to the evolution of the slab's stiffness (as the tangent to the load–deflection curve) during the loading process (see Fig. 7d). However, to monitor the tensile strains on the longitudinal steel bars, several strain gauges were installed on the tensile steel bars in the central zone of the tested slabs, but some of these strain gauges were damaged during the handling and transportation of the slabs. Hence, the recorded tensile strains on the steel bars (by the undamaged strain gauges) were not reported in this study. The SLS conditions for this experimental program were, moreover, adopted according the requirements of the actual European design recommendations ($L/250 = 9.5$ mm, where L is the slab's span and is obtained by $L = 2.R_s$, $R_s = 1186$ mm is the radius of slab, see Fig. 2) [21].

The normalized energy absorption (E_a) and ductility (μ_d) indexes for the strengthened slabs are depicted in Fig. 7c. The normalized means that the registered energy absorption and ductility indexes are divided by the corresponding values recorded for the unstrengthened slab. The energy absorption (E_a) is determined by integrating the area under the load-deflection curve up to the deflection at maximum load carrying capacity (δ_u), while the ductility (μ_d) index is defined as the ratio between the deflection corresponding to the maximum load carrying capacity (δ_u) and to the steel yield initiation (δ_y). Fig. 7c evidences that the Str. A and Str. B slabs provided an enhancement of 70% and 40% in terms of energy absorption capacity, respectively, when compared to the UnStr. slab. However, for the same comparison purpose in terms of ductility index, the Str. A slab provided an increase of about 20%, while a decrease of about 20% was observed by the Str. B slab.

The influence of the CFRP strengthening configuration A and B on the evolution of stiffness during the loading process of the RC slabs was also investigated. The slab's stiffness was calculated as the tangent to the load–deflection curve, and the relationship between the load and normalized stiffness of the tested slabs is depicted in Fig. 7d, where normalized means that the stiffness of the RC slabs is divided by the initial uncracked stiffness of the UnStr. slab. This figure evidences that the strengthened slabs provided higher initial stiffness compared to the corresponding stiffness in the UnStr. slab. Just after crack initiation ("micro-cracks detection" in Fig. 7d), an abrupt decrease of the stiffness was observed in all the tested slabs, and then, an almost constant normalized stiffness was determined in the cracking phase ("meso-cracks detection" in Fig. 7d) up to the steel yield initiation (red markers in the figure). After the steel yielding stage, all the slabs showed a decrease of the stiffness up to the ultimate stage. This decrease of the stiffness was observed with a delay in the strengthened slabs due to their higher load capacities at the steel yield initiation compared to the unstrengthened slab. Moreover, by increasing the CFRP strengthening ratio, the decay of the stiffness after the steel yielding was more gradual up to the ultimate stage.

The average deflection profiles of the tested slabs during the loading process recorded by seven LVDTs positioned along the centerline in both slab directions (exhibited in Fig.8d) is represented in Fig. 8a-c. For the unstrengthened slab (UnStr. in Fig.8a), the deflection values along the centerline at the maximum load had an almost linear variation from the central deflection to the edge deflection. However, for the strengthened slabs (Str. A and Str. B in Figs. 8b and 8c), the deflections around the column area (loading point) had a more gradual decay compared to the other zones along the centerline, due to the higher stiffness provided by the strengthening systems.

3.2. Internal Strain Distribution

The relationship between the load versus tensile strains recorded by the strain gauges installed on the laminates (see Figs. 4 and 5) is depicted in Figs. 9a and 9b for the slabs strengthened using CFRP configuration A and B, respectively. Fig. 9 evidences that in both strengthened slabs, the CFRP tensile strains recorded by symmetric strain gauges in both slab directions (x and y directions in Figs. 4 and 5) have almost similar values, confirming an almost symmetric behavior of the tested slabs in both directions. Fig. 9b, moreover, shows a higher tensile strain value for the strain gauges installed on the central part of the U-shape laminates applied according to the NSM technique compared to the strain values recorded by the strain gauges installed on the extremities of the corresponding U-shape laminates applied according to the ETS technique. This fact can be attributed to the predominant flexural cracking on the slab, prior to the occurrence of the punching shear failure.

3.3. Crack Patterns and Failure Modes

The crack pattern on the tensile surfaces of all the tested slabs at the ultimate stage is shown in Fig. 10. The cracks in all the slabs were initiated at the center point of the slab (loading point) and then, by increasing the load, these cracks propagated toward the supports (flexural cracks). Besides these flexural cracks, after the concrete crack initiation, the punching shear cracks, moreover, were initiated from the compression face of the slab at the loading zone and extended through the depth of the slab up to its tensile surface. By extending the punching cracks, shear failure can, in general, occur outside or within the strengthened zone. In the current experimental program, the unstrengthened slab and the slab strengthened using CFRP configuration B failed in punching with a high concentration of punching shear cracks in the central area. For the Str. B slab, the punching failure occurred outside the strengthened zone at the ultimate stage (see Fig. 10). This punching fracture outside the strengthened zone had a typical circular shape.

On the other hand, regarding the slab strengthened with CFRP configuration A, by increasing the load, after rupturing the ETS part of some U-shape CFRP laminates, punching shear failure occurred within the strengthened zone (represented in Fig. 10). The occurrence of this punching failure within the strengthened zone can be attributed to the lower CFRP reinforcement ratio of the Str. A slab. In other words, the CFRP configuration A did not provide adequate resistance to transfer the shear force to the out of the strengthened zone. Consequently, this slab showed a lower punching strength than the one corresponding to the occurrence of punching failure outside the strengthened zone. However, after initiation of punching crack within the strengthened zone of the Str. A slab, due to the shear resistance of ETS part of U-shape CFRP laminates and the dowel effect of NSM CFRP laminates, a larger cracked area was observed in this slab compared to the other ones, contributing to a more ductile behavior of the Str. A slab. Accordingly, from the observed results in the strengthened slabs, it can be concluded that by increasing the CFRP reinforcement ratio into a certain strengthened area, the susceptibility of occurrence of punching shear failure within the strengthened zone decreases, which can result in a higher punching shear capacity.

4. NUMERICAL SIMULATIONS OF THE EXPERIMENTAL TESTS

4.1. Numerical Model Description

A three dimensional (3D) finite element (FE) approach, capable of simulating the nonlinear behavior of the used materials, was adopted to predict the behavior of RC slabs strengthened with CFRP reinforcements failing in flexure or punching shear. This 3D FE model is available in the FEM-based computer program FEMIX, by modeling one quarter of the tested slab, taking into account its double symmetry (Fig. 11a) to reduce the computational time of the numerical simulations. Fig. 11 represents the FE mesh of the UnStr. Slab, as well as the corresponding support and loading conditions according to the characteristics of the test setup. Two support conditions regarding the experimental test supports ($U_z = 0$) and the ones to ensure the symmetry conditions ($U_x = 0$ and $U_y = 0$) were numerically defined (Figs. 11b and 11c).

Eight-node serendipity solid elements with 2×2×2 Gauss-Legendre integration scheme were used for the concrete. An appropriate element aspect ratio (close to unity) of FE mesh was adopted in order to have acceptable accuracy regarding the mesh density. On the other hand, the 3D multi-directional fixed smeared crack model, described in detailed elsewhere [19, 28], was selected to simulate the concrete's nonlinear behavior considering the fracture mode I and II. In this context, a trilinear diagram, represented in Fig. 12, was adopted to simulate the crack initiation and the fracture mode I propagation of plain concrete [28]. This trilinear diagram defines the fracture mode I modulus ($D_{I,i}^{cr}$), considering the α_i and ξ_i parameters that define the shape of the tensile softening of concrete in terms of the crack's normal stress versus normal strain diagram. Furthermore, the ultimate crack strain ($\varepsilon_{n,u}^{cr}$) is defined as a function of the parameters of the α_i and ξ_i, tensile fracture energy (G_f^I), tensile strength ($f_{ct} = \sigma_{n,1}^{cr}$), and the crack bandwidth (l_b) [28]. In this regard, the present approach uses the concept of concrete crack band width to assure that the results are independent of mesh refinement. For both fracture mode I and II processes, the crack band widths are based on the element geometry and integration points, and are estimated to be equal to the cube root of the volume of the integration point [28]. However, more research is needed to assess the influence of the crack band width parameter on the predictive performance of the behavior of elements failing in shear [29]. According to this multi-directional fixed smeared crack model, a new crack is arisen in an integration point when the angle formed between the new crack and the already existing cracks exceeds a certain threshold angle (α_{th} , a parameter of the constitutive model that in general ranges between 30º and 60º [28]).

Regarding the fracture mode II, the degradation of crack shear stress transfer after concrete crack initiation is simulated using the shear-softening diagram represented in Fig. 13. The initial linear phase of this diagram is defined by the initial shear fracture modulus ($D_{t,1}^{cr}$) and the peak crack shear strain ($\gamma_{t,p}^{cr}$). In this respect, the inclination of the hardening branch of diagram ($D_{t,1}^{cr}$) is introduced according to the following equation:

$$D_{t,1}^{cr} = \frac{\beta}{1-\beta} G_c \tag{1}$$

where G_c is the concrete elastic shear modulus; and β is the shear retention factor, as a constant value in the rang]0,1[[19, 30].

Moreover, the ultimate crack shear strain ($\gamma_{t,u}^{cr}$) depends on the crack shear strength ($\tau_{t,p}^{cr}$), shear fracture energy ($G_{f,s}$), and on the crack bandwidth (l_b) [19]. Concerning the remaining variables of this constitutive model, more details can be found elsewhere [19, 28, 29].

The longitudinal steel bars and CFRP laminates were perfectly bonded to the concrete by embedding 3D two-node cable elements with a 2 Gauss-Legendre integration scheme into the concrete elements. Fig. 11d shows the numerical model of the longitudinal steel bars of the UnStr. Slab using the embedded cable elements. The tensile behavior of the longitudinal steel reinforcement is modeled using a quadrilinear relationship up to its ultimate tensile strength based on the model recommended by [28], while the tensile behavior of the CFRP laminates was assumed to be linear up to its ultimate tensile strength.

4.2. Parameters for the Constitutive Material Models

Regarding the numerical simulation of the tested slabs using the introduced FE model, this section presents the adopted values for the parameters of the constitutive material models. The mechanical properties of the steel bars and CFRP laminates were directly obtained from the relevant experimental material properties tests, whose values are indicated in Table 1.

Table 3 includes the values of the parameters used to define the concrete's constitutive post-cracking laws depicted in Figs. 12 and 13. The tensile strength ($\sigma_{n,1}^{cr}$) and fracture energy (G_f^I) of concrete is obtained by following the recommendations of CEB-FIP Model Code by taking its average compressive strength. The values of the parameters that define the shape of the trilinear crack normal stress versus crack normal strain, α_i and ξ_i, were obtained using inverse analysis by fitting the numerical response of the unstrengthened slab to the corresponding experimental one as much as possible, and the obtained parameter values were kept constant for the numerical simulation of the strengthened slabs.

Besides, since no available experimental results exist to characterize the crack shear softening diagram (Fig. 13), the adopted values, in terms of the crack shear strength ($\tau_{t,p}^{cr}$), shear fracture energy ($G_{f,s}$), and the shear retention factor (β), were also obtained by inverse analysis similar to the adopted strategy for the concrete tensile softening parameters. The value of threshold angle (α_{th}) was assumed to be 30º in the current numerical simulations based on the recommendation of [28].

4.3. Predictive Performance of the Numerical Simulations

The comparison of the applied load versus deflection at the center of all the tested slabs obtained experimentally and numerically is depicted in Fig. 14. This figure indicates a good predictive performance of the FE model in terms of the load-deflection response of the tested slabs. In the cases of the strengthened RC slabs, at the load corresponding to the maximum capacity of the unstrengthened slab, the numerical load-deflection relationship of these strengthened slabs presents a clear increase of the deflection. At this load level the CFRP laminates have avoided the formation of the punching failure surface since they restrict the opening and sliding of this potential failure surface, contributing to maintain highly effective the concrete aggregate interlock resisting mechanisms. Furthermore, the CFRP laminates share with the steel reinforcement the applied stress field, which contribute to decrease the maximum tensile strains in the steel reinforcement and, therefore, to postpone its yield initiation for later stages of the loading process. By bridging effectively the potential punching failure surfaces, the CFRP laminates have promoted the formation of a more diffuse crack patterns (Fig. 10), as was also captured by the numerical simulations (Fig. 14), with a consequent increase of the slab's load carrying capacity.

The good predictive performance of the model in the simulations of this type of structures is also revealed in terms of strains in the CFRPs, as demonstrated in Fig. 15. It is verified that CFRP laminates are only activated after concrete crack initiation, as expected, and the gradient of strains in the central part of the CFRP laminates was higher than in the extremities, due to the predominant flexural reinforcement resisting mechanism of these laminates. The anchorage resisting mechanisms assured by the extremities of the new CFRP laminates were, however, very effective in avoiding premature detachment if only conventional CFRP laminates have been used.

5. NUMERICAL PARAMETRIC STUDY

The current section aims to numerically evaluate the influence of the characteristics of the used strengthening materials on the load-deflection response of the strengthened RC slab by using the described FE model. The analyzed parameters were the cross sectional area, elasticity modulus, and ultimate tensile strength of the CFRP reinforcement. For this purpose, the numerical response of the RC slab strengthened using CFRP configuration B (FE_Str. B) was adopted for the comparison and evaluation purposes.

Fig. 16a compares numerically the load versus center deflection relationship of the RC slabs strengthened using CFRP configuration B with elasticity modulus of 65 GPa and 265 GPa, which is almost 0.4 and 1.6 times the CFRP elasticity modulus adopted in the experimental program (165 GPa), respectively. This figure evidences that the slab's stiffness increases with the CFRP elasticity modulus, while above a certain limit it has no benefits in terms of slab's ultimate load carrying capacity, resulting in a reduction in terms of the ultimate deflection capacity of the strengthened slab.

On the other hand, the numerical response of the RC slabs strengthened using CFRP configuration B with the ultimate tensile strength of 1500 MPa and 2200 MPa (which is almost 0.50 and 0.75 times the adopted ultimate tensile strength in the experimental program (2900 MPa), respectively) is compared in Fig. 16b with the response of the FE_Str. B slab. This figure shows that the RC slab's ultimate load carrying capacity decreases with the ultimate tensile strength of the CFRP reinforcement (it should be noted that perfect bond between CFRP and surrounding concrete substrate is assumed, with the capacity of mobilizing the full tensile capacity of the CFRP systems).

Fig. 16c shows the influence of the cross sectional area of the CFRP reinforcement on the response of the RC slabs in terms of load versus center deflection relationship. For the comparison purposes, the CFRP laminates with cross sectional area of 1.4×15 mm^2 and 1.4×20 mm^2, designated as Str. B_b$_f$15 and Str. B_b$_f$20, respectively, were numerically adopted for the strengthening of the RC slab with similar CFRP arrangements to the Str. B slab (see Fig. 16d for the adopted CFRP cross sectional area). Fig. 16c evidences that the slab's stiffness increases with the CFRP cross sectional area. Above a certain cross sectional area limit a detrimental effect in terms of ultimate deflection and no benefits with reference to the slab's ultimate load carrying capacity are visible. On this point, since the punching failure of these analyzed slabs occur outside the strengthened zone, above a certain cross sectional area limit of FRP reinforcement, it provides no benefits with respect to the slab's ultimate load carrying capacity.

6. ANALYTICAL PREDICTION OF PUNCHING CAPACITY

Regarding the analytical prediction of the punching strength of the RC slabs strengthened using U-shape CFRP laminates, the simplified critical shear crack theory (CSCT), proposed by Muttoni (2008) [31], was modified in order to be applicable for the strengthened slabs considering the concepts of equivalent effective tensile stress ($f_{se,eq}$, Eq. (2b)), equivalent elasticity modulus ($E_{s,eq}$, Eq. (2c)), and equivalent reinforcement effective depth (d_v , Eq. (2d)). According to this theory, the slab's load-rotation relationship is simplified by assuming the rotation (ψ) as a function of the ratio of $(V/V_{flex})^{3/2}$:

$$\psi = 1.5\frac{r_s}{d_v}\frac{f_{se,eq}}{E_{se,eq}}(V/V_{flex})^{3/2} \qquad (2a)$$

where

$$f_{se,eq} = \frac{A_{sl} \cdot f_{sy} + A_{fl} \cdot \frac{E_f}{E_s} . f_{fe}}{A_{sl} + A_{fl} \cdot \frac{E_f}{E_s}} \tag{2b}$$

$$E_{s,eq} = \frac{A_{sl} . E_s + A_{fl} \cdot \frac{E_f}{E_s} . E_f}{A_{sl} + A_{fl} \cdot \frac{E_f}{E_s}} \tag{2c}$$

$$d_v = \frac{d_s . A_{sl} . + d_f . A_{fl} \cdot \frac{E_f}{E_s}}{A_{sl} + A_{fl} \cdot \frac{E_f}{E_s}} \tag{2d}$$

where r_s is radius of circular isolated slab element; f_{sy}, E_s and d_s are the yielding strength, elasticity modulus and effective depth of the flexural steel reinforcement, respectively; f_{fe} , E_f and d_f are the effective tensile stress, elasticity modulus and internal arm of the FRP reinforcement, respectively; V and V_{flex} are the applied shear force and the shear force associated with flexural capacity of the slab considering the participation of the FRP that can be obtained using the simplified model proposed by [32] for predicting the behavior of RC elements strengthened with FRP reinforcement, respectively; A_{sl} and A_{fl} are the cross sectional area of flexural steel and FRP reinforcement in the slab strip (introduced in section 2.1), respectively.

According to the CSCT model proposed by Muttoni (2008), the failure criterion to calculate the shear strength of slab is determined by the following equation:

$$V_R = \frac{3}{4} \frac{b_0 . d_v . \sqrt{f_c^{'}}}{1 + 15 . \frac{\psi . d_{s,eq}}{d_{g0} + d_g}} \tag{4}$$

b_0 is the perimeter of the critical section located $d_v/2$ from the face of the column; $f_c^{'}$ is the concrete compressive strength; d_g is the maximum aggregate size and d_{g0} is a reference aggregate size of 16 mm.

By considering the equivalent effective depth (d_v), the ACI 318-08 expression (Eq. (5)) was, moreover, adopted for the determination of the punching shear capacity of the strengthened slabs [33].

$$V_R = \min \begin{cases} 0.33 b_0 . d_v . \sqrt{f_c^{'}} \\ 0.083 \left(\dfrac{\alpha_s . d_v}{b_0} + 2 \right) b_0 . d_v . \sqrt{f_c^{'}} \\ 0.17 \left(\dfrac{2}{\beta_c} + 1 \right) b_0 . d_v . \sqrt{f_c^{'}} \end{cases} \tag{5}$$

where α_s is a constant of 40 for interior columns, 30 for edge columns, and 20 for corner columns; and β_c is the ratio of long side to short side of the column.

On the other hand, the recommendation of Eurocode 2 was, also, used to determinate the punching shear capacity of the strengthened slabs using the following equation [21]:

$$V_R = 0.18 b_{0e} . d_v . \xi (100 . \rho_{eql} . f_c^{'})^{1/3} \;\; \rightarrow \; \xi = 1 + \sqrt{\frac{200\, mm}{d_v}} \leq 2.0 \tag{6}$$

where b_{0e} is the perimeter of the critical section located $2.d_v$ from the face of the column; ρ_{eql} is the equivalent reinforcement ratio that can be obtained by:

$$\rho_{eql} = \rho_{sl} + \frac{E_f}{E_s} \rho_{fl} \tag{7}$$

The punching shear capacity of all the tested RC slabs were analytically determined using the proposed formulations, and the relevant results are compared in Fig. 17 and in Table 4 with the experimentally obtained. This table evidences that regarding the strengthened slabs, all the used analytical approaches had a good predictive performance, while concerning to the unstrengthened slab, the proposed model by Muttoni (2008) results in more accurate prediction compared to the recommendations of ACI 318-08 and Eurocode 2.

7. CONCLUSIONS

The current work has explored the potentialities of a novel hybrid technique for the simultaneous flexural and punching shear strengthening of existing RC slabs using innovative U-shape CFRP laminates. Furthermore, a 3D nonlinear finite element (FE) approach was developed to numerically simulate these types of structures. From the obtained results, the following conclusions can be pointed out:

- Strengthening the RC slabs using the conventional and U-shape CFRP laminates provided an average increase in terms of load carrying capacity at concrete cracking (43%), steel yielding (43%), and service conditions (27%), when the corresponding load capacities of the unstrengthened slab are considered for the comparison purposes. Moreover, this strengthening technique increased significantly the punching shear capacity of the unstrengthened RC slab (with an average increase of 40%). The aforementioned load capacities had a higher tendency to increase with the CFRP reinforcement ratio.

- All the tested slabs failed by punching shear failure within or outside of the flexural-shear strengthened zone of the slabs without observing the CFRP deboning or concrete cover detachment failures, resulting in the anchorage benefits for the U-shape CFRPs. By increasing the CFRP reinforcement ratio into a constant flexural-shear strengthened area, the susceptibility of occurrence of punching shear failure within the strengthened zone decreases, favoring the increase of the punching shear capacity.

- The ultimate deflection of the strengthened slabs decreased with the increase of the CFRP reinforcement ratio. These results, which imply a decrease in terms of the ductility and energy absorption capacities with the CFRP reinforcement ratio, suggest the adoption of a limit of CFRP reinforcement ratio to assure a sufficient degree of ductility and energy absorption indexes.

- A 3D FE model, capable of simulating the nonlinear behavior of the constituent materials, was developed to simulate the behavior of RC slabs strengthened with the proposed CFRP hybrid technique. The good predictive performance of the FE model in terms of predicting the response of hybrid CFRP strengthened RC slabs was demonstrated. Moreover, the prevailing failure modes of the slabs at the maximum load carrying capacity (punching shear failure) were numerically predicted similar to the ones experienced experimentally. Hence this FE model provides the possibility to do trial and error to optimize the efficiency of these types of CFRP hybrid techniques for the simultaneous flexural and shear strengthening of RC slabs before their real application, considering their load carrying and deflection capacities.

- From the numerical parametric studies, it was verified a tendency for the increase of the slab's stiffness and load carrying capacity when the elasticity modulus and cross sectional area of the CFRP laminates increase, but above a certain limit the ultimate deflection of the slab is detrimentally affected. The slab's ultimate load carrying capacity increases with the tensile strength of the CFRP laminates, but the slab's stiffness is not affected by this property of the CFRP laminates.

- Regarding the analytical prediction of the punching capacity of the RC slabs strengthened with U-shape CFRPs, the formulations proposed by Muttoni (2008), ACI 318-08 and Eurocode 2 were modified considering the concepts of equivalent effective tensile stress, equivalent elasticity modulus, and equivalent reinforcement ratio and its corresponding effective depth. The obtained results evidenced that all the modified analytical approaches had a good performance to predict the punching capacity of the RC slabs strengthened with U-shape CFRPs.

8. ACKNOWLEDGEMENTS

The authors acknowledge the financial support provided by QREN (through the Operational Program COMPETE) in the scope of the CutInov Project (n. 38780) involving the Clever Reinforcement Company and the Structural Composites Research group of ISISE-Minho University.

9. REFERENCES

[1] Adom-Asamoah M, Kankam C. Behaviour of reinforced concrete two-way slabs using steel bars milled from scrap metals. Materials & Design, 2008, 29:1125-30.

[2] Moreno C, Ferreira D, Bennani A, Sarmento A, Noverraz M. Punching shear strengthening of flat slabs: cfrp and shear reinforcement. Concrete – Innovation and Design, fib Symposium, Copenhagen May 18-20, 2015.

[3] Ju M, Park C, Hwang E, Sim J. Predictability evaluation of the existing punching shear formulas using failure test and probability-based approach. KSCE Journal of Civil Engineering, 2015, 19:1420-30.

[4] Gardner N, Huh J, Chung L. Lessons from the Sampoong department store collapse, Cement and Concrete Composites. 2002, 24:523-9.

[5] Sissakis K, Sheikh S. Strengthening concrete slabs for punching shear with carbon fiber-reinforced polymer laminates. ACI Structural Journal, 2007, 104:49.

[6] Rezazadeh M. Innovative methodologies for the enhancement of the flexural strengthening performance of NSM CFRP technique for RC beams. University of Minho, PhD Thesis, Guimaraes, Portugal, 2015.

[7] Rezazadeh M, Costa I, Barros J. Influence of prestress level on NSM CFRP laminates for the flexural strengthening of RC beams. Composite Structures, 2014, 116:489-500.

[8] El-Hacha R, Rizkalla S. Near-surface-mounted fiber-reinforced polymer reinforcements for flexural strengthening of concrete structures. ACI Structural Journal, 2004, 101.

[9] Rezazadeh M, Cholostiakow S, Kotynia R, Barros J. Exploring New NSM Reinforcements for the Flexural Strengthening of RC Beams: Experimental and Numerical Research. Composite Structures, 2016, 141:132–145.

[10] Breveglieri M, Aprile A, Barros J. Embedded Through-Section shear strengthening technique using steel and CFRP bars in RC beams of different percentage of existing stirrups. Composite Structures, 2015, 126:101-13.

[11] Meisami M, Mostofinejad D, Nakamura H. Punching shear strengthening of two-way flat slabs using CFRP rods. Composite Structures, 2013, 99:112-22.

[12] Koppitz R, Kenel A, Keller T. Punching shear strengthening of flat slabs using prestressed carbon fiber-reinforced polymer straps. Engineering Structures, 2014, 76:283-94.

[13] Esfahani M, Kianoush M, Moradi A. Punching shear strength of interior slab–column connections strengthened with carbon fiber reinforced polymer sheets. Engineering Structures, 2009, 31:1535-42.

[14] Faria D, Einpaul J, Ramos A, Ruiz M, Muttoni A. On the efficiency of flat slabs strengthening against punching using externally bonded fibre reinforced polymers. Construction and Building Materials, 2014, 73:366-77.

[15] Rezazadeh M, Ramezansefat H, Barros J. NSM CFRP Prestressing Techniques with Strengthening Potential for Simultaneously Enhancing Load Capacity and Ductility Performance. Journal of Composites for Construction(ASCE), 2016, DOI: 10.1061/(ASCE)CC.1943-5614.0000679.

[16] Genikomsou A, Polak M. Finite element analysis of punching shear of concrete slabs using damaged plasticity model in ABAQUS. Engineering Structures, 2015, 98:38-48.

[17] Teixeira M, Barros J, Cunha V, Moraes-Neto B, Ventura-Gouveia A. Numerical simulation of the punching shear behaviour of self-compacting fibre reinforced flat slabs. Construction and Building Materials, 2015, 74:25-36.

[18] Youm K, Kim J, Moon J. Punching shear failure of slab with lightweight aggregate concrete (LWAC) and low reinforcement ratio. Construction and Building Materials, 2014, 65:92-102.

[19] Ventura-Gouveia A. Constitutive models for the material nonlinear analysis of concrete structures including time dependent effects. University of Minho, PhD Thesis, Guimaraes, Portugal, 2011.

[20] Baghi H, Barros J, Ventura-Gouveia A. Shear strengthening of reinforced concrete beams with hybrid composite plates. Journal of Advances in Structural Engineering, 2016, DOI: 0.1177/1369433215622873.

[21] EN1992-1-1. Design of concrete structures—Part 1-1: General rules and rules for buildings.: Eurocode 2: de Normalisation, Comité Européen; 2004.

[22] Barros J, Neto B, Melo G, Frazão C. Assessment of the effectiveness of steel fibre reinforcement for the punching resistance of flat slabs by experimental research and design approach. Composites Part B: Engineering. 2015, 78:8-25.

[23] ACI-440.2R. Guide for the Design and Construction of Externally Bonded FRP Systems for Strengthening Concrete Structures. American Concrete Institute (ACI) Committee 440, 2008.

[24] Barros, J., Dias, S. Near surface mounted CFRP laminates for shear strengthening of concrete beams. Cement and Concrete Composites Journal. 2006, 28(3), 276-292.

[25] Rezazadeh M, Baghi H, Barros J, Laranjeira J. Exploring the potentialities of a new type of CFRP laminate for the simultaneous flexural and shear strengthening of RC beams: numerical research. The 12th International Symposium on Fiber Reinforced Polymers for Reinforced Concrete Structures (FRPRCS-12) & The 5th Asia-Pacific Conference on Fiber Reinforced Polymers in Structures (APFIS-2015) Joint Conference, Nanjing, China, 2015.

[26] EN-10002-1. Metallic materials - Tensile testing, Part 1: Method of test at ambient temperature. European Standard, CEN; 1990.

[27] ASTM-D3039. Standard method for tensile properties of polymer matrix composite materials, American Society for Testing and Materials (ASTM); 2000.

[28] Sena-Cruz J. Strengthening of concrete structures with near-surface mounted CFRP laminate strips. University of Minho, PhD Thesis, Guimaraes, Portugal, 2004.

[29] Barros J, Baghi H, Dias S, Ventura-Gouveia A. A FEM-based model to predict the behaviour of RC beams shear strengthened according to the NSM technique. Engineering Structures, 2013, 56:1192-206.

[30] Behbahani A, Barros J, Ventura-Gouveia A. Plastic-damage smeared crack model to simulate the behaviour of structures made by cement based materials. International Journal of Solids and Structures, 2015, 73:20-40.

[31] Muttoni A. Punching shear strength of reinforced concrete slabs without transverse reinforcement. ACI structural Journal. 2008, 105: 440-450.

[32] Rezazadeh M., Barros J., Costa I. Analytical approach for the flexural analysis of RC beams strengthened with prestressed CFRP. Composites Part B: Engineering, 2015, 73: 16-34.

[33] ACI-318-08. Building Code Requirements for Structural Concrete. American Concrete Institute (ACI) Committee 318, 2008.

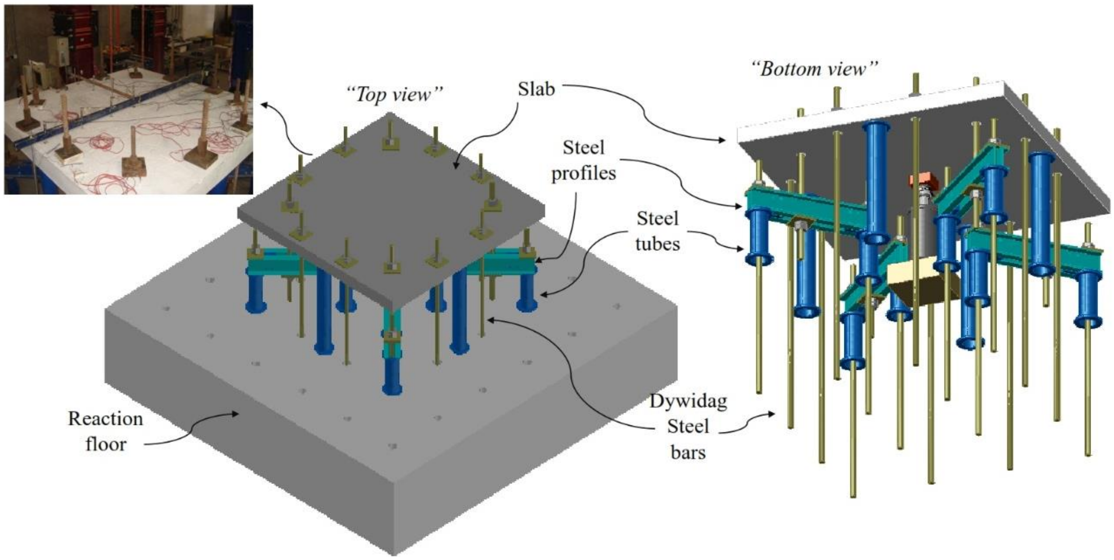

Fig.1: The loading configuration and support conditions of the tested slabs

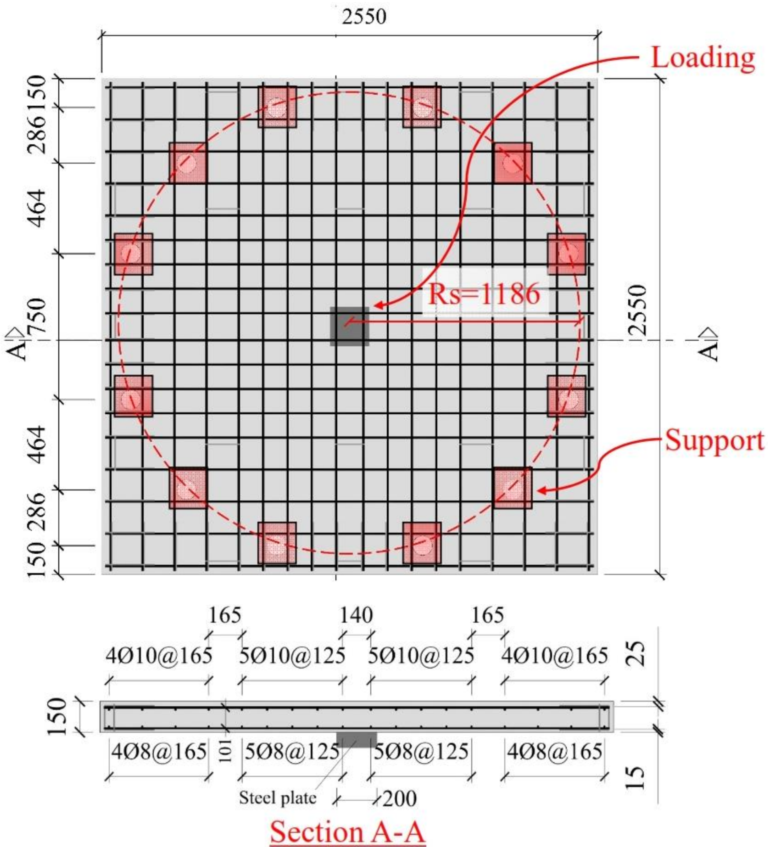

Fig. 2: The geometry and steel reinforcement details of the tested slabs (dimensions in mm).

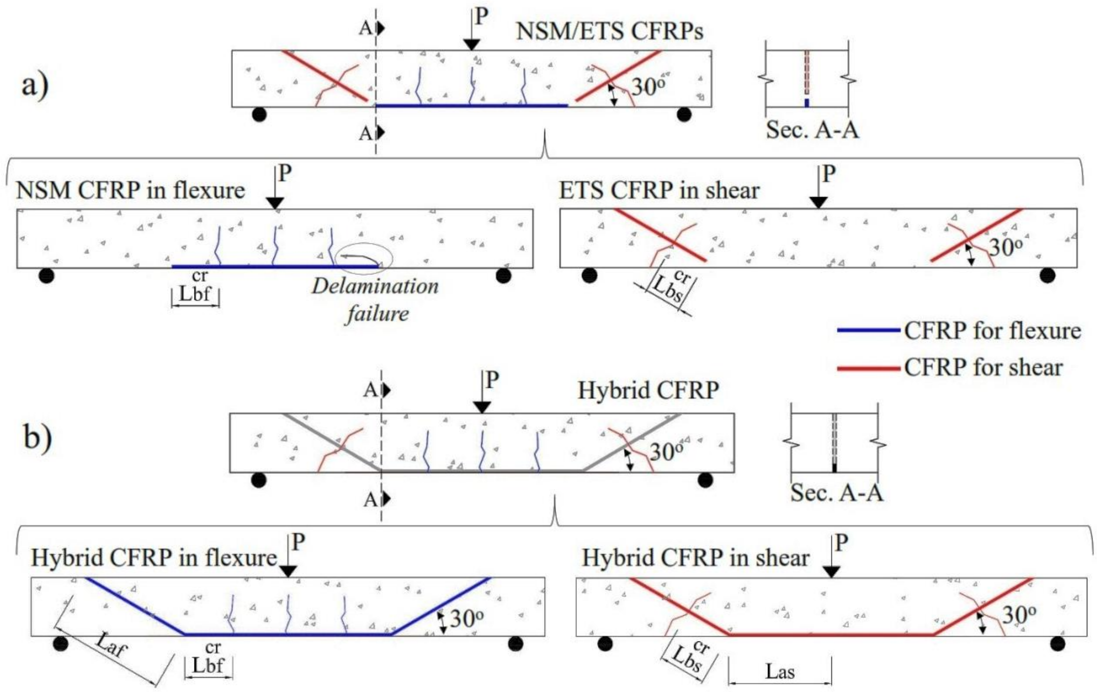

Fig. 3: a) Separate application of NSM and ETS CFRP laminates, b) application of hybrid CFRP laminates

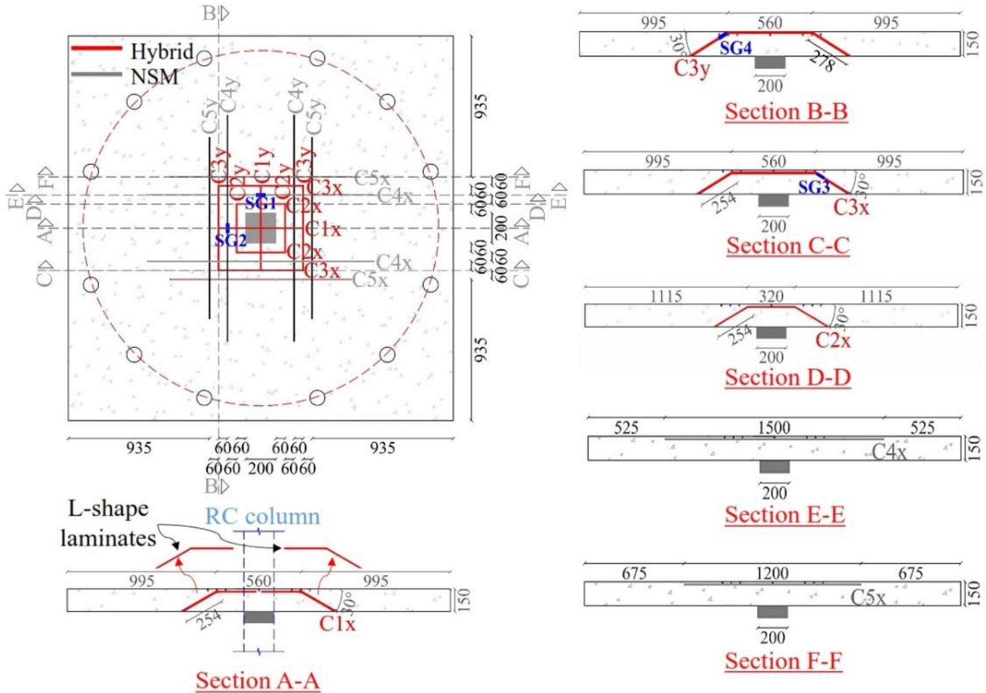

Fig. 4: CFRP strengthening configurations of Str. A slab (dimensions in mm)

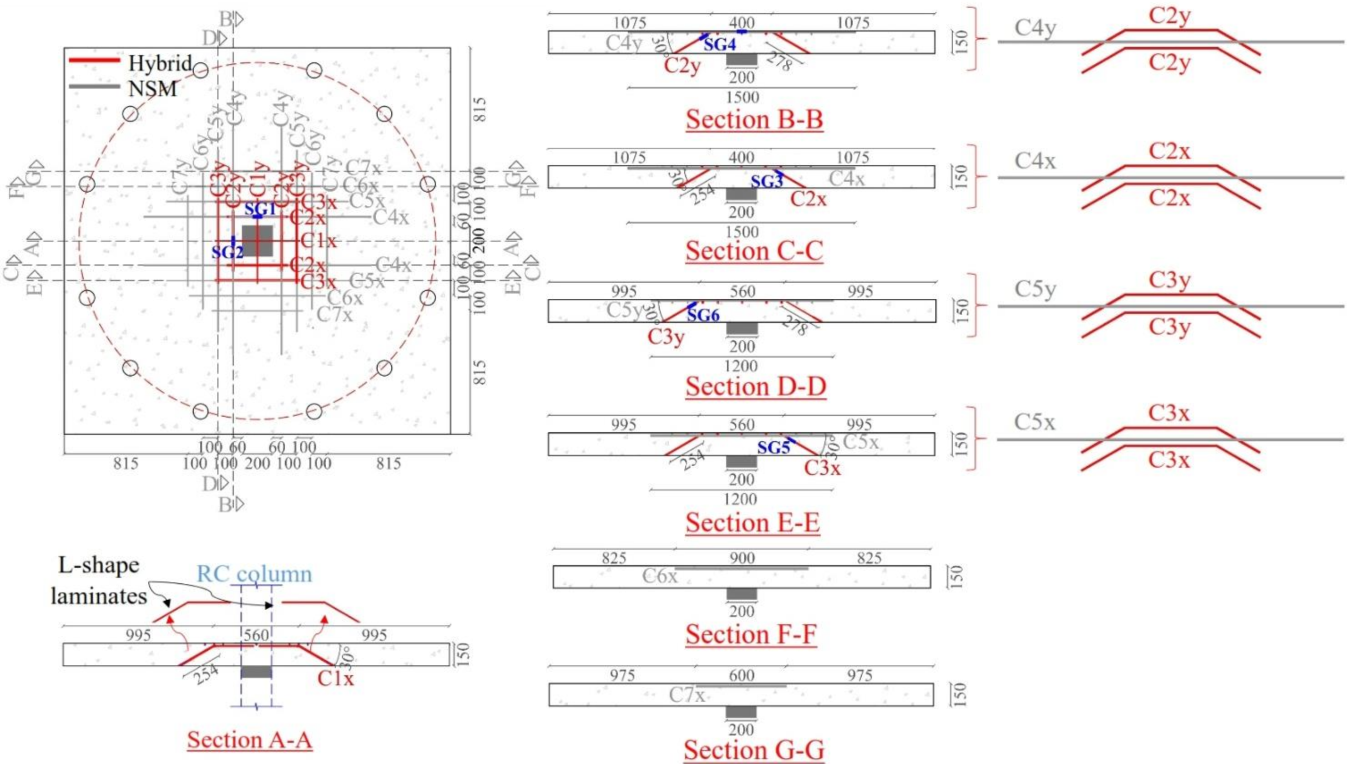

Fig. 5: CFRP strengthening configurations of Str. B slab

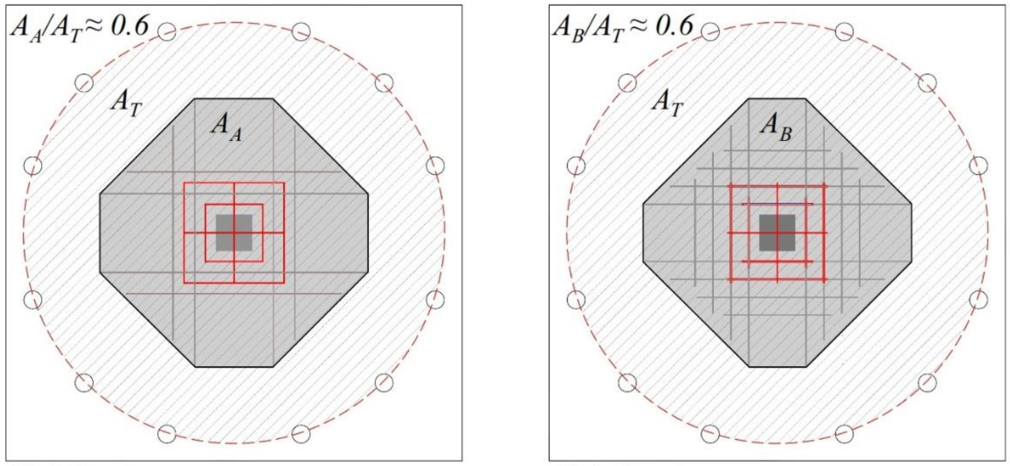

Slab Str. A *Slab Str. B*

Fig. 6: Flexural-shear strengthened zone of CFRP configuration A and B

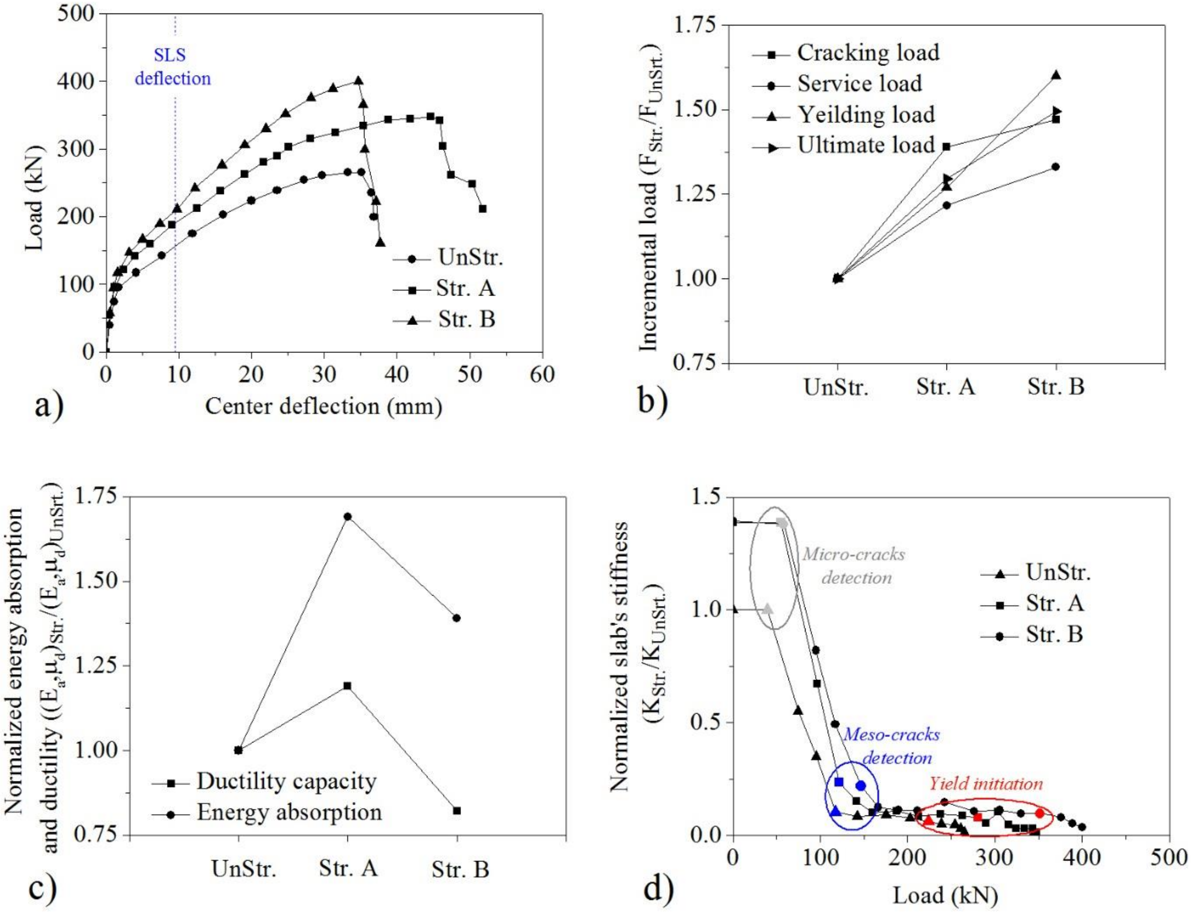

Fig. 7: a) The applied load versus deflection at the center of slabs, b) increment of load capacities, c) normalized energy absorption and ductility capacities, d) normalized tangential slab's stiffness

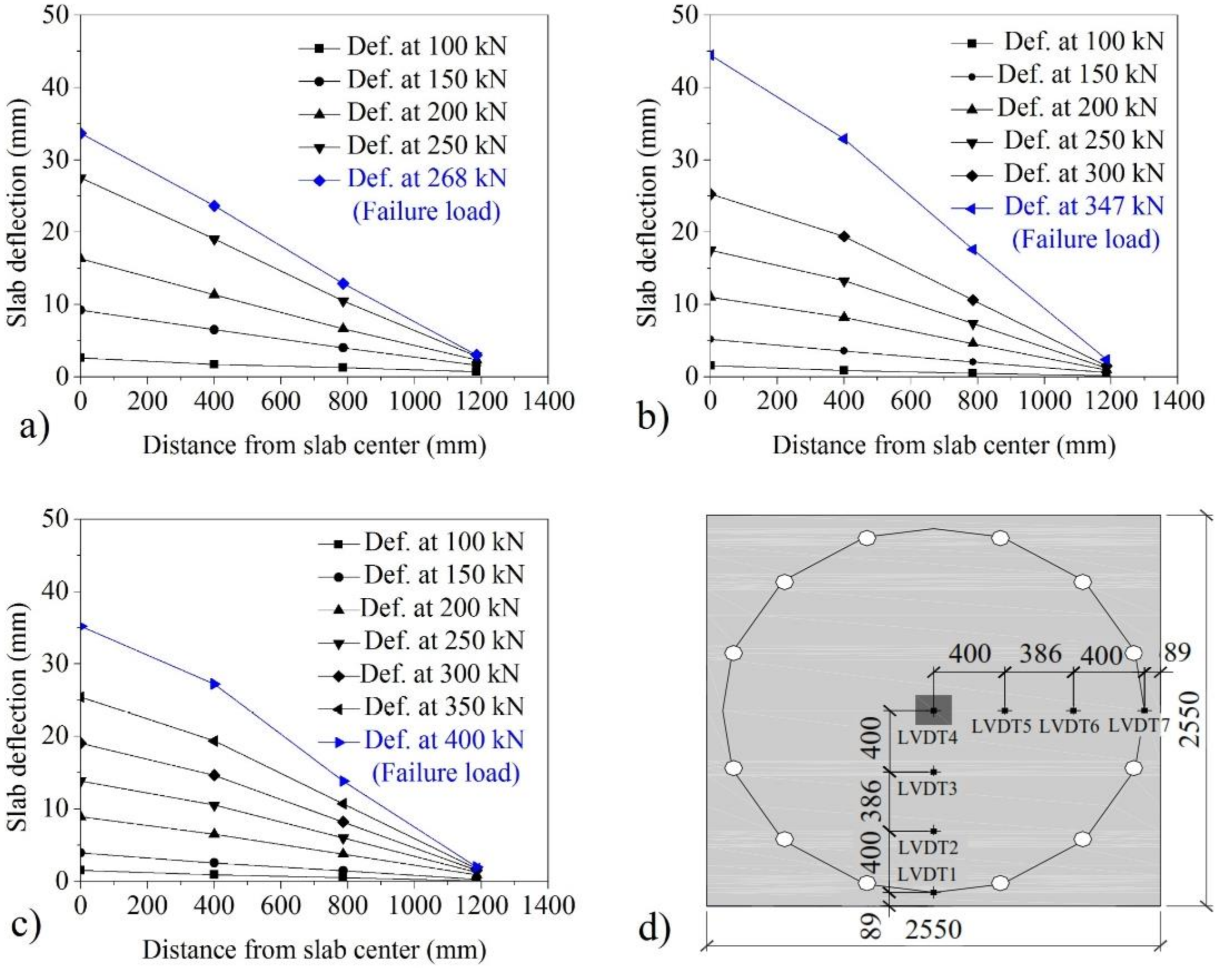

Fig. 8: The average deflection profiles of: a) UnStr. Slab, b) Str. A slab, c) Str. B slab, d) position of LVDTs (dimensions in mm)

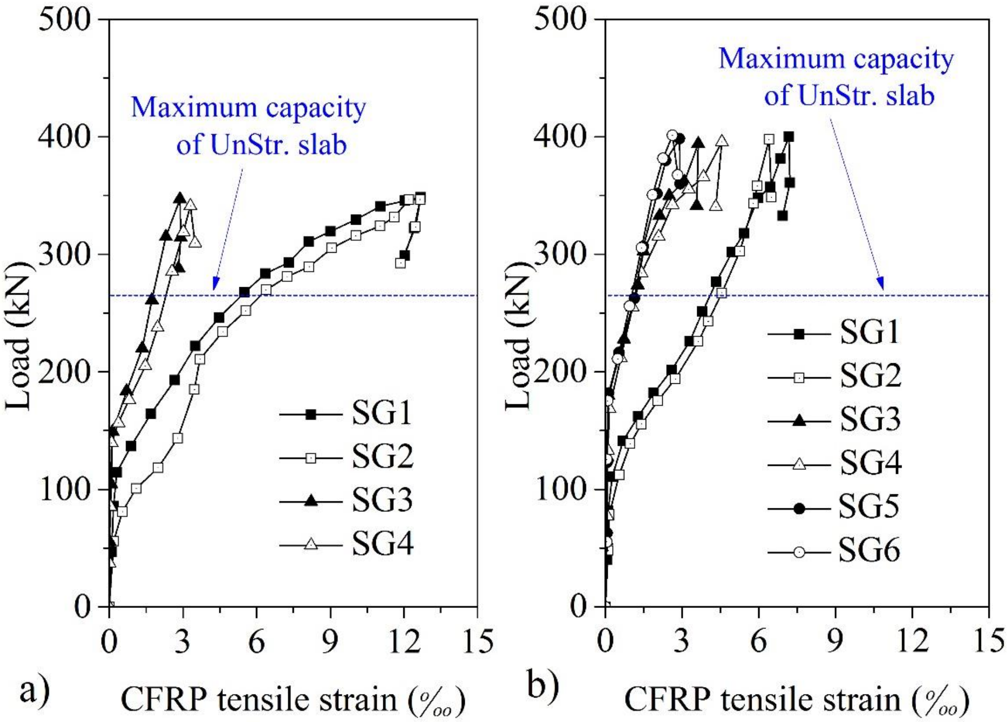

Fig. 9: CFRP tensile strains recorded by the strain gauges: a) Str. A slab, b) Str. B slab

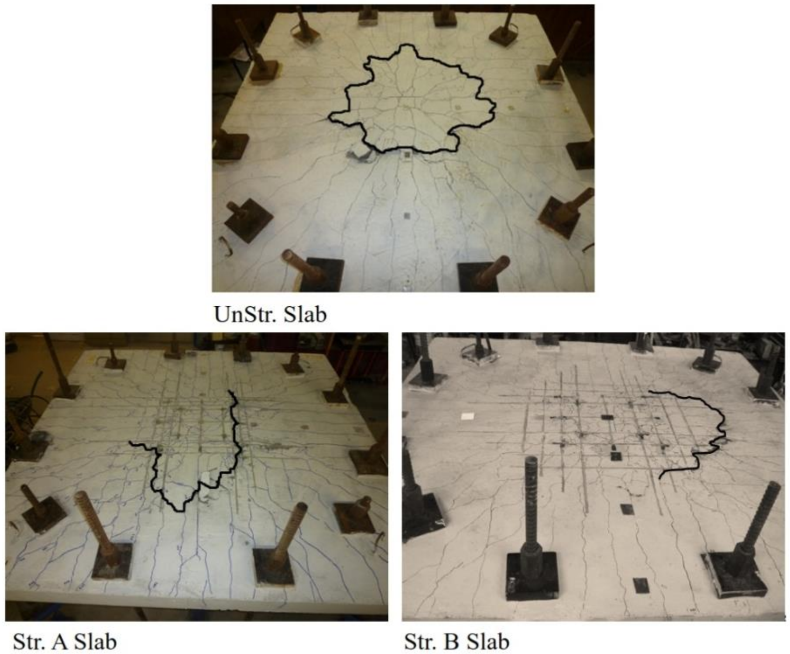

Fig. 10: The crack pattern on the tensile surfaces of all the tested slabs at the ultimate stage

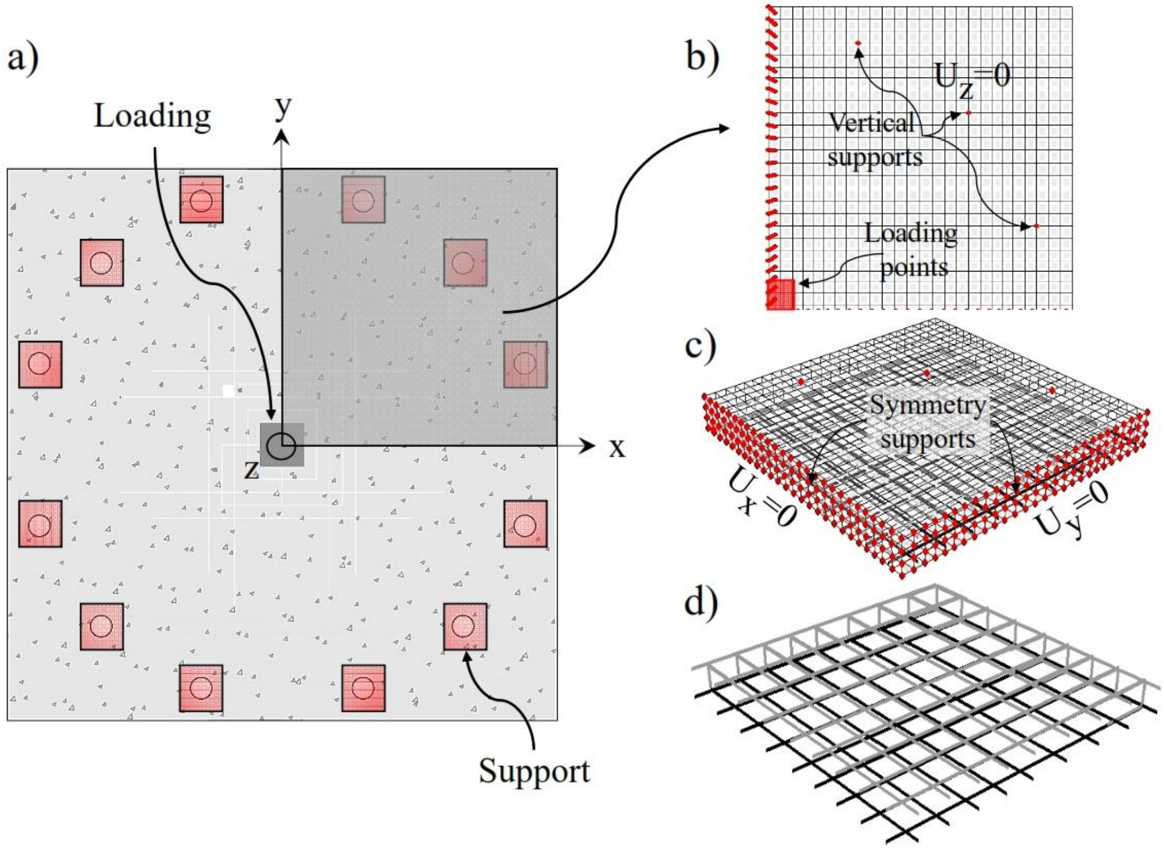

Fig. 11: a) Double symmetry planes, b) FE mesh, and support and loading conditions, c) symmetry supports, d) steel reinforcements

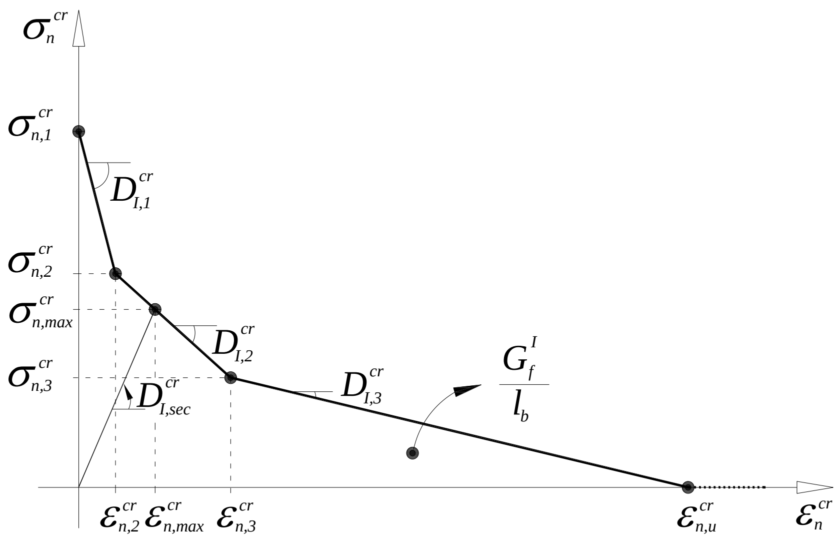

Fig. 12: Trilinear stress-strain diagram of the fracture mode I crack propagation ($\sigma_{n,2}^{cr} = \alpha_1 \sigma_{n,1}^{cr}$, $\sigma_{n,3}^{cr} = \alpha_2 \sigma_{n,1}^{cr}$, $\varepsilon_{n,2}^{cr} = \xi_1 \varepsilon_{n,u}^{cr}$, $\varepsilon_{n,3}^{cr} = \xi_2 \varepsilon_{n,u}^{cr}$)

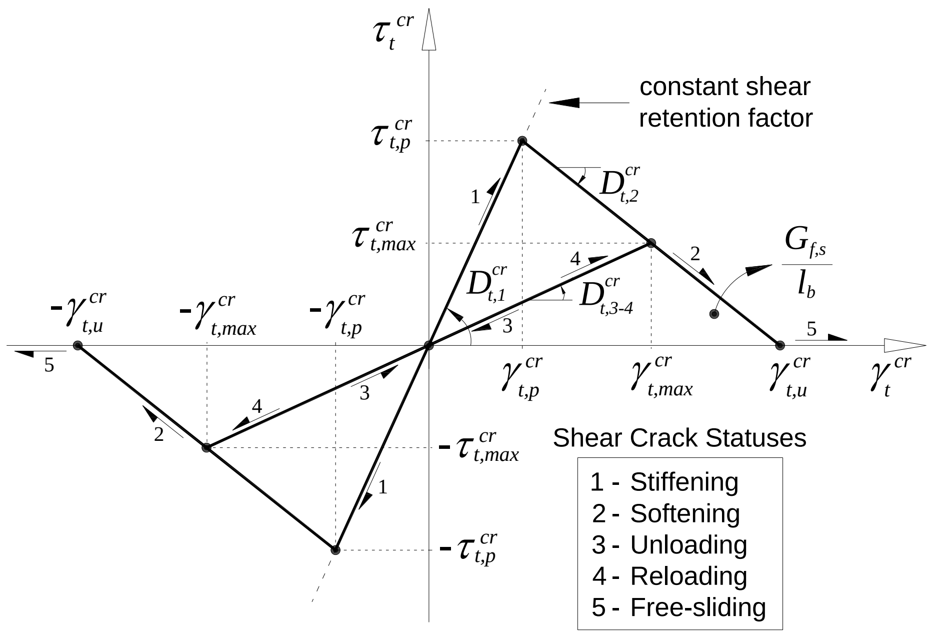

Fig. 13: Stress-strain diagram of the fracture mode II

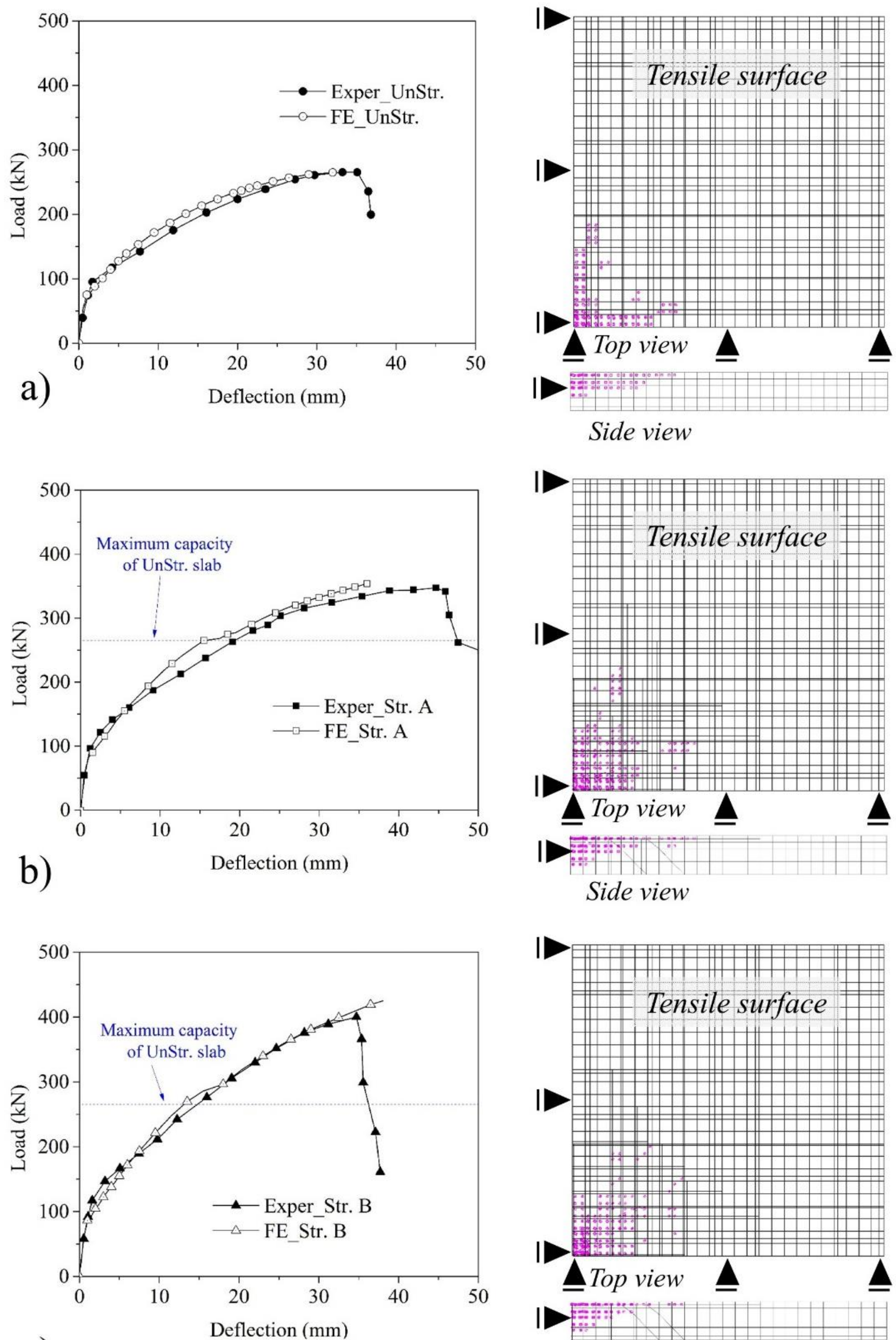

Fig. 14: Assessment of the predictive performance of the FE model in terms of load-deflection relationship and crack patterns: a) UnStr. Slab, b) Str. A slab, c) Str. B slab

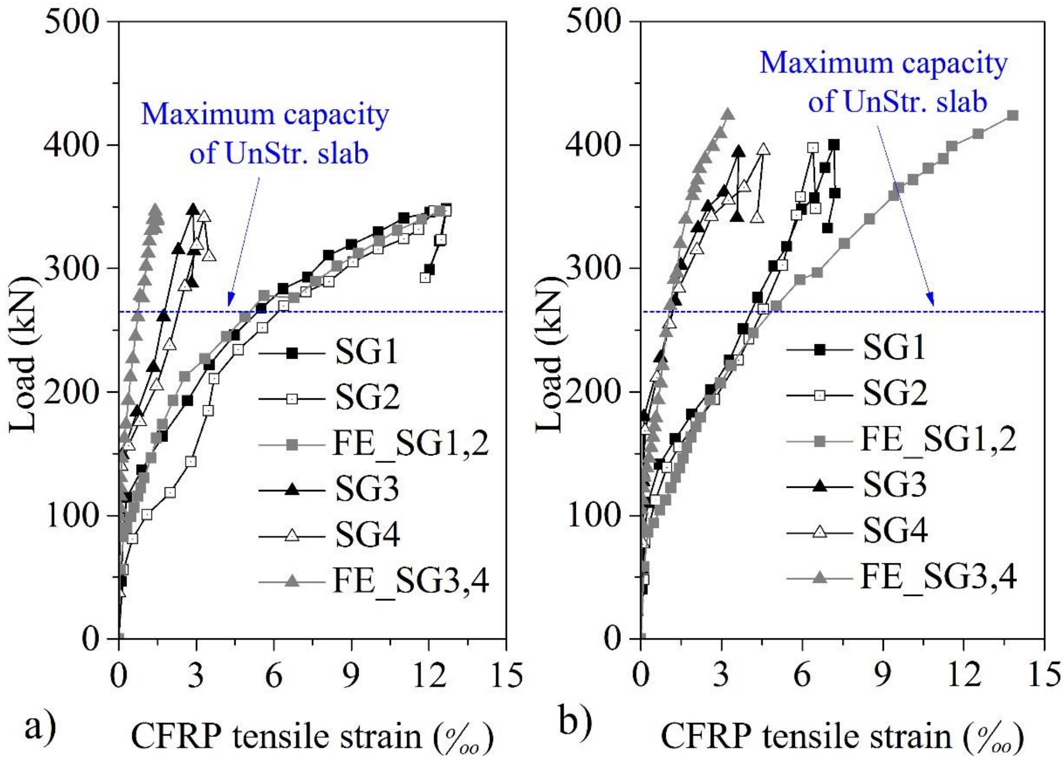

Fig. 15: Assessment of the predictive performance of the FE model in terms of load-CFRP tensile strain relationship: a) Str. A slab, b) Str. B slab

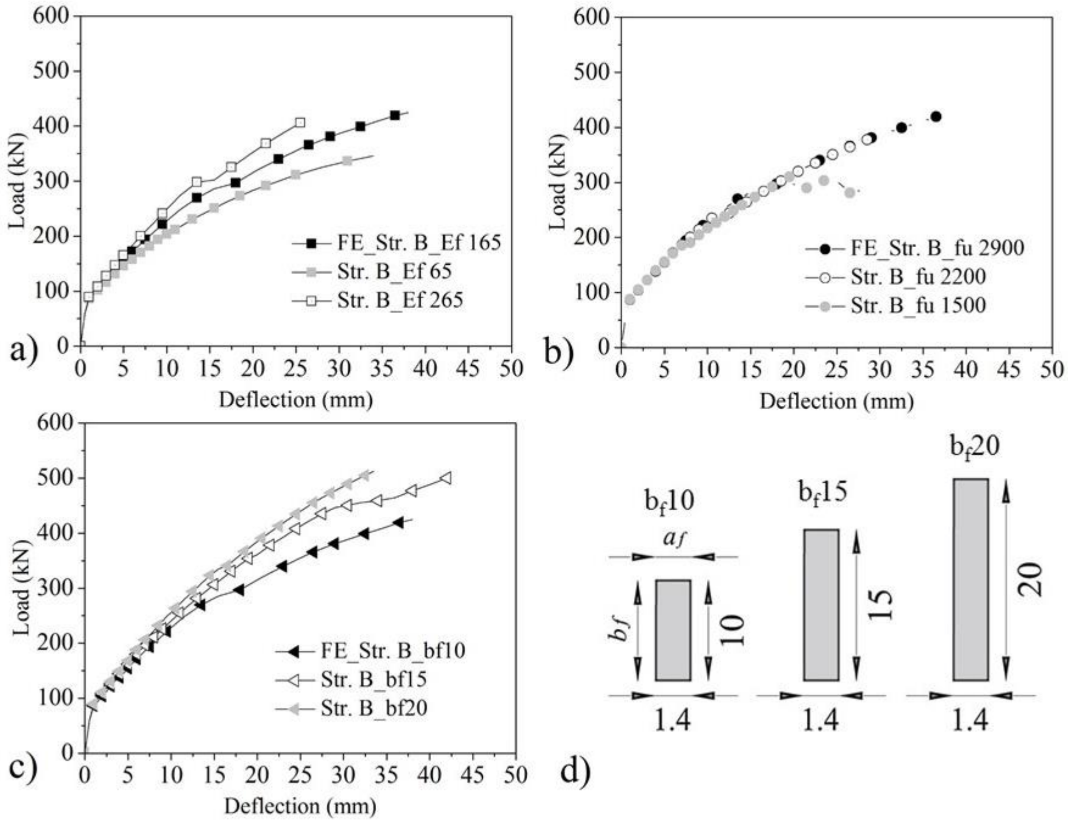

Fig. 16: The influence of the relevant parameters on the behavior of the RC slabs: a) elasticity modulus of CFRP, b) CFRP ultimate tensile strength, c) CFRP cross sectional area, d) geometric characteristic of CFRP laminates

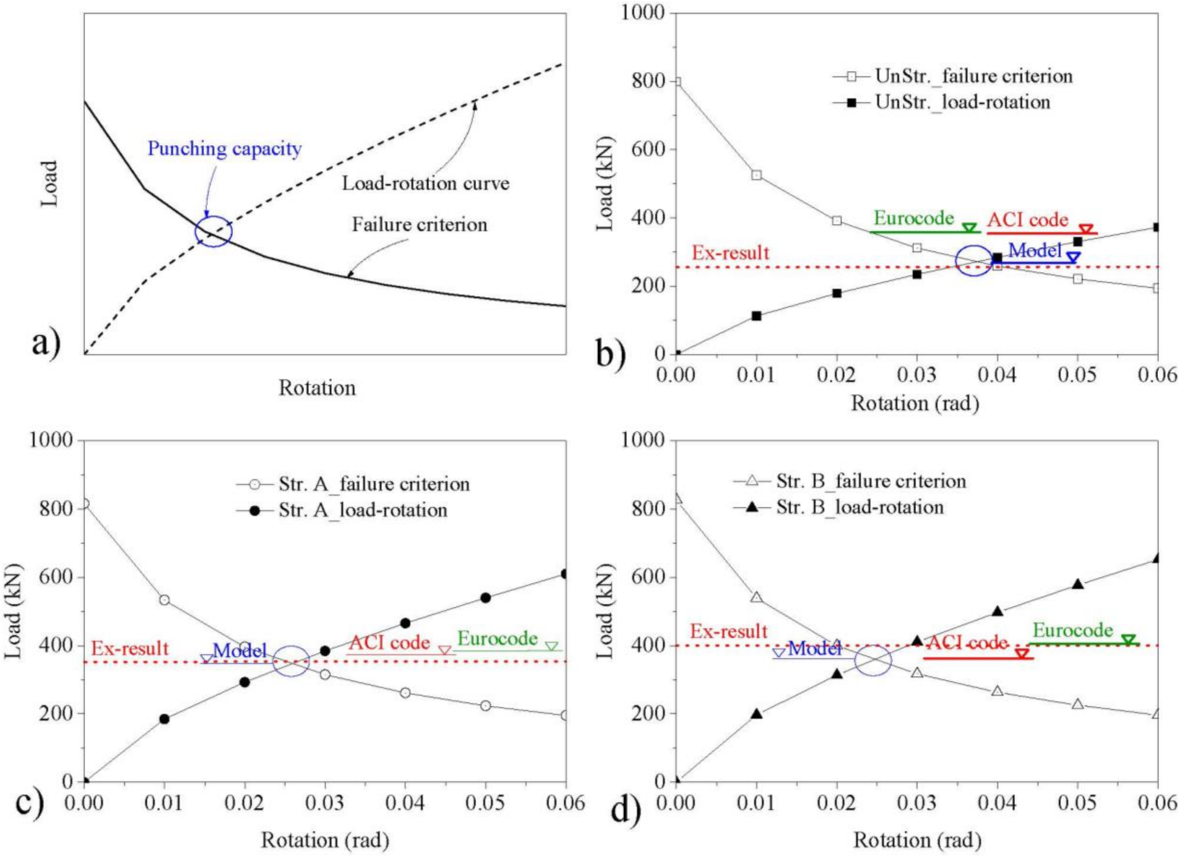

Fig. 17: a) Schematic representation for determining the punching shear capacity, analytical prediction of the punching strength of the slabs: b) UnStr., c) Str. A, d) Str. B

Table 1. The average values of the main properties of the constituent materials

Materials	Main Properties						
	f'_{cm} (MPa)	E_c (GPa)	f_{sym} (MPa)	f_{sum} (MPa)	E_f (GPa)	f_{fum} (MPa)	ε_{fu} (‰)
Concrete	43.0	31.8	-	-	-	-	-
Steel bars (ϕ8)	-	-	545.9	680.1	-	-	-
Steel bars (ϕ10)	-	-	530.6	646.4	-	-	-
CFRP laminate	-	-	-	-	165.5	2896.5	17.5

f'_{cm} and E_c: concrete compressive strength and its Young's modulus, f_{sym} and f_{sum}: yield and ultimate strengths of steel bars, E_f, f_{fum}, and ε_{fu}: elasticity modulus, tensile strength, and ultimate tensile strain of CFRP.

Table 2. Relevant results obtained in the tested slabs

Tested RC slabs	P_{cr} (kN)	δ_{cr} (mm)	P_y (kN)	δ_y (mm)	P_u (kN)	δ_u (mm)	P_{SLS} (kN)
UnStr.	39.4	0.46	220	19.5	268.0	33.14	158.5
Str. A	54.8	0.47	280	21.7	347.3	44.02	191.4
Str. B	58.1	0.54	351	24.8	400.9	34.46	211.5

P_{cr} and δ_{cr} are the load and deflection at cracking initiation; P_y and δ_y are the load and deflection at yielding of tensile bars; P_u and δ_u are the maximum load and corresponding deflection; P_{SLS} is the load at SLS conditions.

Table 3. The adopted values for the concrete constitutive model

Property	Value
Poisson's ratio (ν_c)	0.15
Initial Young's modulus (E_c)	31800 MPa
Tri-linear tension-softening diagram	$\sigma_{n,1}^{cr}$ = 2.9 MPa; G_f = 0.08 N/mm ξ_1 = 0.005; α_1 = 0.3; ξ_2 = 0.2; α_2 = 0.1
Parameter defining the mode I fracture energy available for the new set of smeared cracks	n = 3
Parameters for defining the crack shear stress-crack shear strain softening diagram	$\tau_{t,p}^{cr}$ = 1.0 MPa; $G_{f,s}$ =0.05 N/mm; β =0.05
Crack bandwidth (l_b)	Cube root of the volume of the integration point
Threshold angle	α_{th} = 30^o
Maximum number of sets of smeared cracks per integration point	2

Table 4. Analytical prediction of the experimental results

RC slabs	P_u^{Ex} (kN)	P_u^{ACI} (kN)	P_u^{Euro} (kN)	P_u^{Model} (kN)	$\frac{P_u^{ACI}}{P_u^{Ex}}$	$\frac{P_u^{Euro}}{P_u^{Ex}}$	$\frac{P_u^{Model}}{P_u^{Ex}}$
UnStr.	268.0	355.2	356.9	271.8	1.33	1.33	1.01
Str. A	347.3	362.5	383.5	338.6	1.04	1.10	0.97
Str. B	400.9	367.5	404.5	361.9	0.92	1.01	0.90
					Ave:1.10	Ave:1.15	Ave:0.96